Available online at www.sciencedirect.com
ScienceDirect
Journal of Organometallic Chemistry 692 (2007) 3461–3473
Journal of Organometallic Chemistry
www.elsevier.com/locate/jorganchem

New platinum(II) complexes as triplet emitters for high-efficiency monochromatic pure orange electroluminescent devices

Gui-Jiang Zhou [a], Xing-Zhu Wang [a,b], Wai-Yeung Wong [a,*], Xiao-Ming Yu [c], Hoi-Sing Kwok [c], Zhenyang Lin [d]

[a] *Department of Chemistry and Centre for Advanced Luminescence Materials, Hong Kong Baptist University, Waterloo Road, Hong Kong, PR China*
[b] *Institute of Polymer Science, College of Chemistry, Xiangtan University, Xiangtan 411105, Hunan Province, PR China*
[c] *Department of Electronic and Electrical Engineering, Centre for Display Research, Hong Kong University of Science and Technology, Clearwater Bay, Hong Kong, PR China*
[d] *Department of Chemistry, Hong Kong University of Science and Technology, Clearwater Bay, Hong Kong, PR China*

Received 19 March 2007; received in revised form 11 April 2007; accepted 11 April 2007
Available online 21 April 2007

Abstract

New multi-component orange phosphorescent platinum complexes [Pt(L)(acac)] (Hacac = acetylacetone, HL = (9,9-diethyl-7-pyridin-2-ylfluoren-2-yl)diphenylamine **1**, (9,9-diethyl-7-pyridin-2-ylfluoren-2-yl)di(*p*-tolyl)amine **2**) were prepared and characterized by spectroscopic and X-ray crystallographic methods. We report the redox and photophysical properties of **1** and **2** and compare these results with the unsubstituted analogue [Pt(L)(acac)] (HL = 9,9-diethyl-2-pyridin-2-ylfluorene **3**). Efficient pure orange-emitting organic light-emitting devices (OLEDs) based on **1** were fabricated. The device performance with 3,5-dicarbazolylbenzene (mCP) as the host can furnish maximium external quantum, current and power efficiencies of 4.65%, 11.75 cd/A and 5.27 lm/W at 7 V, respectively. The device with 4,4′-*N*,*N*′-dicarbazolebiphenyl (CBP) as the host can perform better with peak external quantum and current efficiencies of 6.64% and 15.41 cd/A at 7.5 V and a power efficiency of 7.07 lm/W at 6.5 V. Unlike the OLEDs made from other cyclometalated Pt(β-diketonato) complexes in which the electroluminescence spectra generally displayed both the monomeric and excimeric emissions with different relative intensities upon variation of dopant concentration, our devices emit a strong pure orange light with stable CIE color coordinates. From a steric point of view, no evidence of low-energy aggregate emission is observed for a doping level up to 12 wt.%. The present work confers a good platform for the realization of robust triplet emitters in the fabrication of highly efficient monochromatic OLEDs through the design of multifunctional chelating ligands.

Keywords: Arylamine; Platinum; Crystal structures; Fluorene; Phosphorescence

1. Introduction

The design and synthesis of transition metal complexes has been recognized as the research focus in the development of organometallic-based optoelectronics, such as light-emitting diodes, chemosensors and photovoltaic dye-sensitized devices [1]. Enormous research work on cyclometalated or oligopyridyl complexes of Ru(II) [2], Os(II) [3], Re(I) [4] and Ir(III) [5] has been pursued over the years for studying their unique photophysical properties which would find vital applications in the aforesaid frontiers. Recently, substantial research was focused on the use of iridium(III) complexes in organic light-emitting diodes (OLEDs) [6,7]. Similarly, the application of platinum(II) complexes chelated with aromatic ligands such as bipyridine, phenanthroline, 2-phenylpyridine, or similar derivatives as electrophosphorescent emitters has recently been demonstrated to impact the development of high-performance monochromatic OLEDs and white OLEDs (WOLEDs) [8,9]. These Pt(II) phosphors are attractive by virtue of their large energy gap between the MLCT or ^{3}LC

* Corresponding author. Tel.: +852 34117074; fax: +852 34117348.
E-mail address: rwywong@hkbu.edu.hk (W.-Y. Wong).

0022-328X/$ - see front matter © 2007 Elsevier B.V. All rights reserved.
doi:10.1016/j.jorganchem.2007.04.013

emissive states (MLCT = metal-to-ligand charge transfer, LC = ligand centered) and high-energy metal-centered (MC) states [10,11]. However, many of these Pt(II) emitters still suffer from many intrinsic obstacles. Among these, for example, the Pt(OEP) (H_2OEP = octaethylporphyrin) displays a ligand-based π–π^* phosphorescence with a long lifetime up to 30–50 μs. Accordingly, saturation of the emission signals and a rapid drop in device efficiency at high driving currents are anticipated. There are also undesirable occasions where their MLCT/^{3}LC and MC states lie too close in energy so that they can thermally equilibrate rapidly, thereby quenching the emission via the fast radiationless decay of the MC states [12]. Furthermore, the open coordination spheres of the square-planar Pt(II) core can allow for other deactivation pathways to occur through metal interactions with the environment [13]. So, they usually display a mixed ^{3}LC/MLCT excited state as well as an aggregate emission band caused by the strong intermolecular interactions, which would broaden the electroluminescence (EL) spectra to result in a poor color purity. Instead these complexes are more frequently employed in the fabrication of white organic light-emitting diodes (WOLEDs) [14,15]. All of these factors essentially contribute to the inferior efficiency of OLEDs and render these Pt(II) complexes less attractive as efficient monochromatic light sources. Therefore, a rational design aimed at the reduction of the phosphorescence radiative lifetime and suppressing the self-aggregation of Pt(II) complexes is needed to exploit the full potential of Pt(II) electrophosphors.

Recently, the issues on carrier-injection in OLEDs arouse much concern, because some of the promising phosphorescent emitters such as those functionalized with fluorene-based chromophores suffer from a large hole-injection (HI) barrier [16,17]. We are interested in looking for some new metal phosphors exhibiting improved HI and hole-transporting (HT) features. In this contribution, we show that the luminescent platinum cores can be incorporated into the multifunctional conjugated organic architectures. The synthesis, redox, photophysical and electroluminescent (EL) properties of these cyclometalated Pt(II) complexes with diarylaminofluorene moiety will be discussed in which HI/HT and EL functional groups are integrated into one molecular unit catering for more efficient charge transport in the EL process. It has been demonstrated that the diarylaminofluorenyl ligand can offer a good resort in facilitating the injection of holes, displaying a pure emission color, enhancing the thermal and morphological stability and weakening the intermolecular interaction in Pt-based triplet emitters that are essential for efficient monochromatic OLEDs.

2. Results and discussion

2.1. Preparation and characterization

The synthetic protocol for the platinum complexes **1**–**3** is shown in Scheme 1. As the key synthons, the fluorene-based organic ligands $\mathbf{HL_1}$, $\mathbf{HL_2}$ and $\mathbf{HL_3}$ were prepared via Stille coupling of (7-bromo-9,9-diethylfluoren-2-yl)diphenylamine, (7-bromo-9,9-diethylfluoren-2-yl)di(*p*-tolyl)amine or 7-bromo-9,9-diethylfluorene with 2-(tributylstannyl)pyridine in the presence of a catalytic quantity of $Pd(PPh_3)_4$. All the Pt(II) complexes were synthesized in two steps from the cyclometalation of K_2PtCl_4 with the organic ligands to form initially the chloro-bridged dimers, followed by chloride cleavage with acetylacetone using Na_2CO_3 [18]. Purification of the mixture by silica chromatography furnished **1**–**3** as air-stable orange to yellow powders in high purity. They were each thoroughly characterized by NMR spectroscopy and FAB-MS to confirm their well-defined chemical structures.

2.2. Crystal structure analyses

Good-quality crystals of **1**–**3** were grown from their respective $CHCl_3$/hexane solutions at room temperature (rt) and characterized using X-ray crystallography (Fig. 1 and Table 1). Intermolecular interactions in the crystal lattices of Pt(II) complexes are known to play a key role in their solid-state emission properties [11,12]. Unlike other relevant Pt complexes in which two molecules exist as a dimer packed in a head-to-tail pattern in the asymmetric unit (3.15–3.76 Å) [9,19], there is only one unique discrete molecule per asymmetric unit among **1**–**3**. The Pt···Pt separation is calculated to be 5.1–7.3 Å, which is too long for any significant Pt–Pt contacts. So, there should be negligible interaction among the molecules of **1**–**3** in the solid state. The structures of **1** and **2** differ from **3** by the presence of a diarylamino core attached to the fluorene ring. All of them have a distorted square planar geometry at the Pt center. The Pt–C bond lengths for **1**, **2** and **3** are 1.969(4), 1.958(3) and 1.973(3) Å, respectively, which are close to the mean value reported [20]. The bond length of Pt–N (1.985(3)–1.997(3) Å) is slightly longer compared to that of common Pt–N bonds, as this N is opposite to the acac O atom having a weak *trans* influence [21]. The Pt–O distances are within the range of 1.994(3)–2.087(3) Å as for other cyclometalated Pt(β-diketonato) derivatives and it is clear that the Pt–O edge *trans* to carbon (2.080(2)–2.087(3) Å) is longer compared to that of the other Pt–O bond (1.995(3)–2.018(3) Å), as the O atom *trans* to carbon has a strong *trans* influence [19,22,23].

2.3. DFT calculations

Density functional theory (DFT) calculations at the B3LYP level were performed on the basis of their experimental geometries from the X-ray data. The HOMO − 1, HOMO and LUMO orbitals for **1**–**3** are shown in Fig. 2. It can be seen clearly that the HOMO and LUMO correspond to the π and π^* molecular orbitals of the conjugated system, respectively. Despite the subordinate contribution from the Pt orbitals, the HOMO is mainly delocalized over the fluorenyl moiety for **1**–**3** and it also extends through the

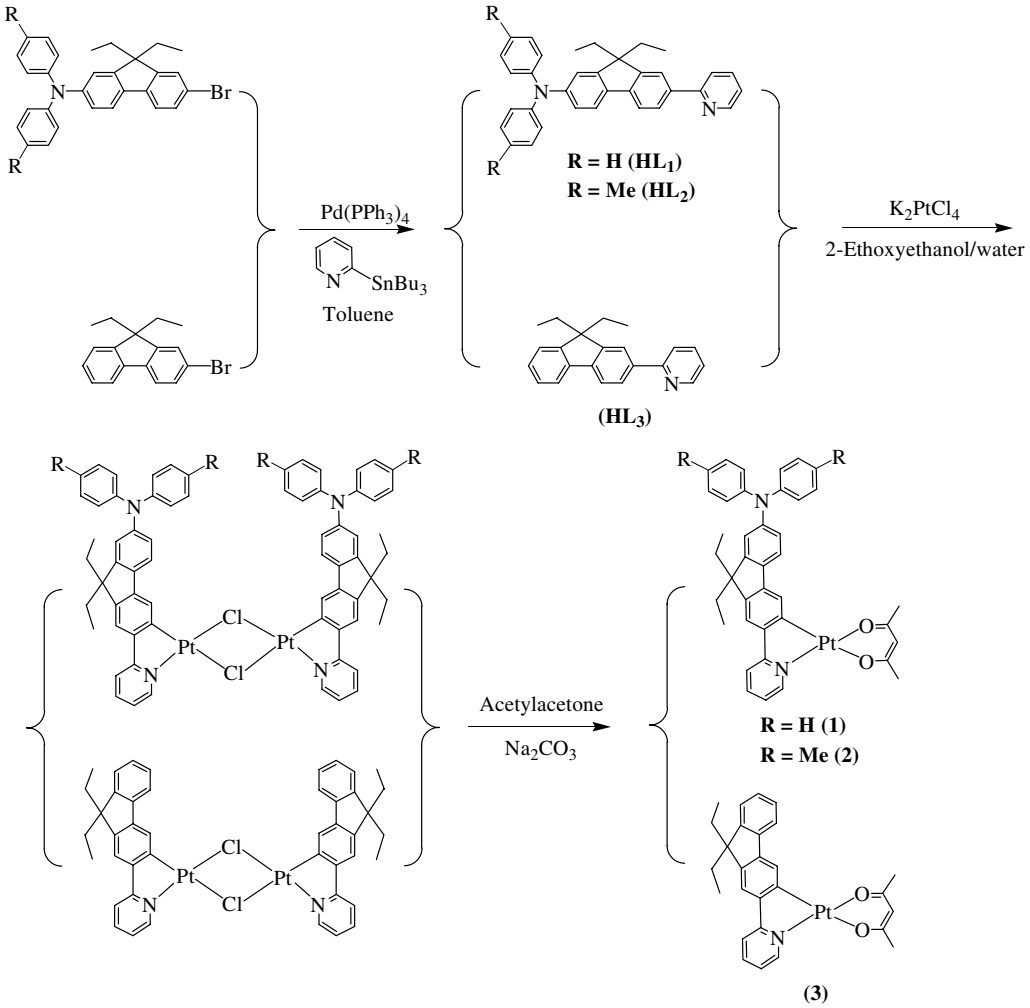

Scheme 1. The synthetic sketches for the platinum complexes **1**–**3**.

diarylamino group in **1** and **2**. In the LUMO, the p_π orbitals from atoms of the pyridyl group make the major contribution although mixing of the p_π orbitals from the fluorenyl moiety can also be clearly seen. On the basis of these computational results, we consider the HOMO–LUMO transitions for **1**–**3** to the LC π–π^* band of the conjugated organic moiety. For **1** and **2**, the transition band also contains a substantial intraligand charge transfer (ILCT) character from the diarylaminofluorenyl unit to the pyridyl ring whereas a MLCT component may be present for **3** because of the metal contribution in the HOMO. In all cases, there is an involvement of Pt orbitals in the HOMO − 1. Our results also show that the NAr_2 groups (Ar = Ph, tol) in **1** and **2**, which are electron-donating, reduce the HOMO–LUMO gap much with respect to **3** (3.13 eV, 3.11 eV and 3.68 eV for **1**–**3**, respectively). However, **1** and **2** display similar energy gaps, signalling that the effect of Me group substitution on the gap lowering is quite small.

Comparing $\mathbf{HL_1}$ and **1**, DFT data shows that the metal coordination does not have a notable change in the orbital characteristics in the frontier orbitals but the presence of metal chromophore lowers the HOMO–LUMO gap significantly. The metal unit pushes up the orbital energy of the HOMO slightly because the metal-bonded fluorenyl moiety in **1**, which makes significant contribution in the HOMO, becomes more electron-rich relative to $\mathbf{HL_1}$. To the LUMO, the metal lowers down its orbital energy because the pyridyl group, which makes the major contribution in the LUMO, becomes less electron-rich after metalation.

2.4. Photophysical and thermal properties

The UV–Vis and photoluminescence (PL) spectra of **1**–**3** are depicted in Fig. 3 and the corresponding data are listed in Table 2. The intense absorption bands below 400 nm appear to be LC transitions since they closely resemble the spectra of the free ligand (see Supporting Information), and are assigned to the spin-allowed $^1\pi$–π^* transitions associated with the arylamino and aminofluorenyl fragments. For **1** and **2**, the absorption bands around 364–387 nm are red-shifted from the free ligand absorptions because of perturbation from the metal but are not solvatochromic. Similar absorption features were also

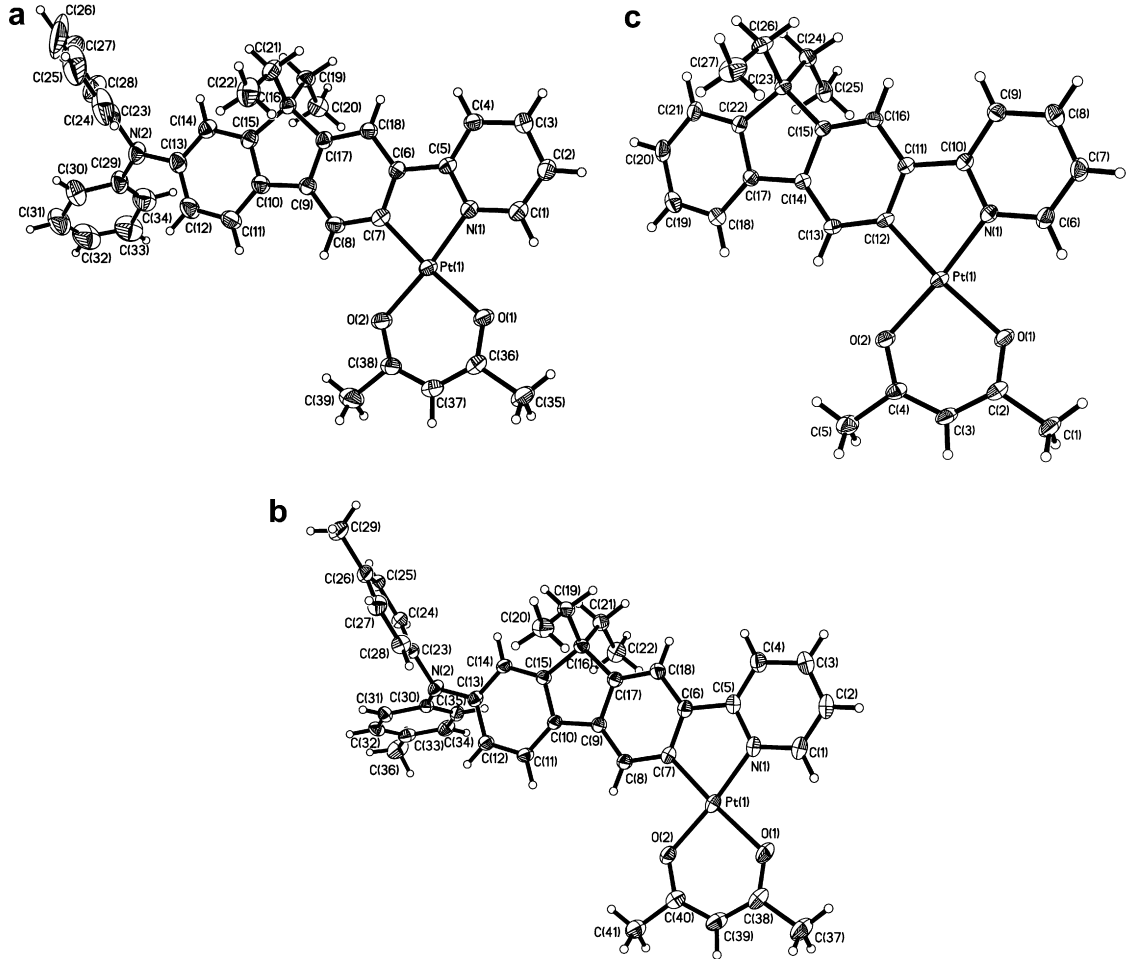

Fig. 1. Perspective drawings of (a) **1**, (b) **2** and (c) **3**.

Table 1
Selected bond lengths (Å) and angles (°) around the metal core in **1**–**3**

	Pt–N	Pt–C	Pt–O	C–Pt–N	O–Pt–O
1	1.990(4)	1.969(4)	2.085(3), 2.018(3)	81.07(17)	92.05(13)
2	1.997(3)	1.958(3)	2.087(3), 1.994(3)	81.88(13)	91.95(11)
3	1.985(3)	1.973(3)	2.080(2), 1.995(3)	81.49(13)	91.89(11)

observed in the spectra of Ar_2N–C_6H_4–X compounds near 300 and 350 nm [24]. Also, the lowest-lying absorption features observed in the visible light region beyond 400 nm for **1** and **2** are solvatochromic ($\lambda_{abs} = 429$, 435 and 447 nm for **1** and 434, 440 and 453 nm for **2** as we decrease the solvent polarity from DMSO to CH_2Cl_2 and CCl_4), indicative of a typical charge-transfer character, and are thus tentatively attributed to an admixture of ILCT and $^3\pi$–π^* excited states. The assignment was supported by theoretical calculations for **1** and **2**, which reveal that the HOMO is basically triarylamine-based and the LUMO predominantly corresponds to the π^* orbitals of the fluorenylpyridine group. However, we cannot totally rule out the possibility of a minor MLCT-type component in the absorption band since the HOMO − 1 level also contains substantial contribution from the Pt's d orbital character (vide supra). While the higher energy absorption peak does not change with the R groups, the lower-lying band is slightly red-shifted by the electron-pushing units ($\lambda_{abs} = 435$ nm for **1** and 440 nm for **2**). For **3**, the intense $^1\pi$–π^* transition at 326 nm is accompanied by weaker, lower energy features with extinction coefficients of 6300–6600 M^{-1} cm^{-1} that probably corresponds to a combination of ^{1}MLCT, ^{3}MLCT, and $^3\pi$–π^* excited states [19]. The triplet character arises from the strong spin–orbital coupling between the singlet and triplet manifolds in such heavy metal complexes, which are commonplace for other similar Pt cyclometalates. This can be corroborated with the DFT results for **3** in which the valence orbital picture consists of concomitant LC and MLCT components in the lowest energy absorption (vide supra). The lowest energy absorption peak of **1** and **2** is located at wavelength ($\lambda_{abs} = 434$ nm for **1** and $\lambda_{abs} = 439$ nm for **2**) longer than that of **3** without the diarylamino units ($\lambda_{abs} = 422$ nm). The introduction of an electron-donating diarylamino group into the electron-deficient pyridine moiety is expected to increase the intramolecular donor–acceptor (D–A) character of the ligand, causing a red-shift of the absorption features. All the Pt complexes show strong emission bands at rt. For **1**, there are two distinguishable

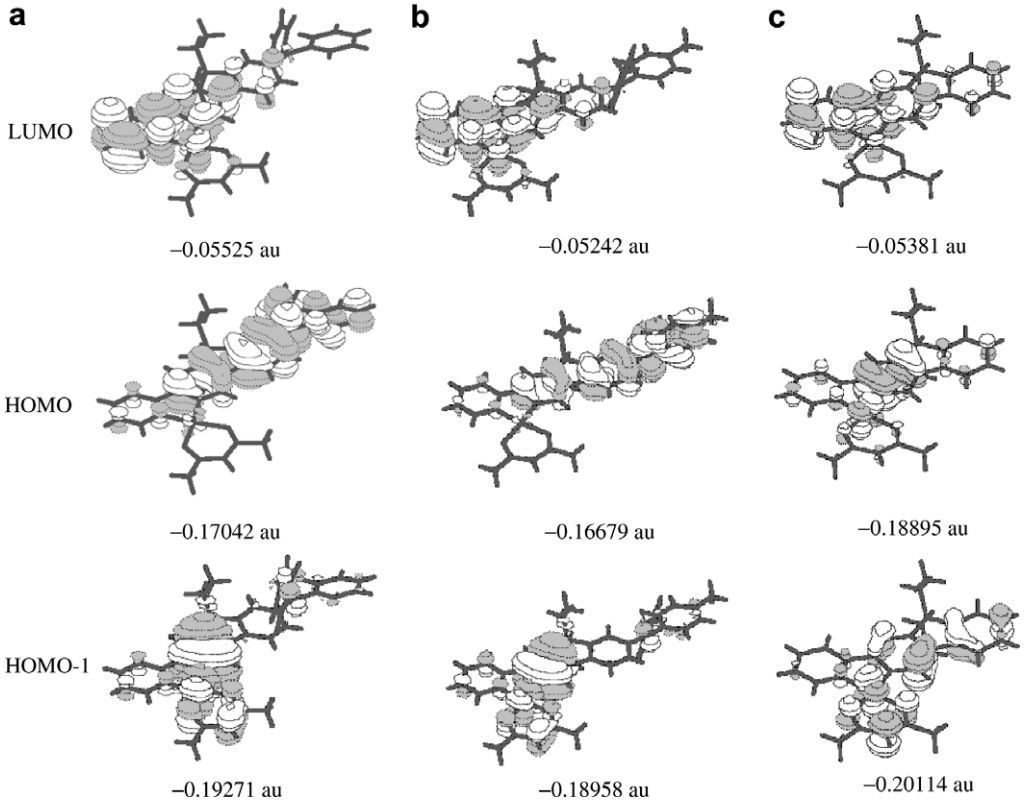

Fig. 2. Contour plots of the frontier molecular orbitals for (a) **1**, (b) **2** and (c) **3**. (1 au = 27.2114 eV).

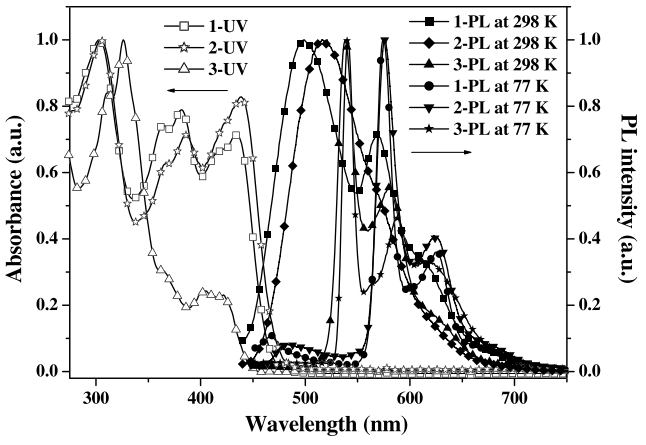

Fig. 3. UV–Vis and photoluminescence spectra of **1**–**3** in CH_2Cl_2.

emission bands in CH_2Cl_2 solution at rt comprising essentially the mixed LC fluorescence and $^3\pi$–π^* phosphorescence. The broad and featureless band at ca. 498 nm should be assigned to the ILCT emission which exhibits a small Stokes shift of ca. 65 nm, a singlet lifetime of 2.52 ns and a usual rigidochromic blue-shift of 30 nm on cooling of the solution sample to 77 K (Fig. 3) [19,25]. However, the band at ca. 569 nm should emanate from the LC $^3\pi$–π^* state for its vibrational fine structure observed and the intensity enhancement at low temperature. Examination of the PL behavior of **1** in the solid-state ($\lambda_{em} = 568$ nm) suggests no fluorescence peak and the absence of aggregate states in the thin neat film (vide infra), consistent with the X-ray structural data where there is no apparent Pt···Pt short contacts. Excitation spectra were also taken for **1** in solution to confirm the

Table 2
Photophysical and thermal data for **1**–**3**

Compound	Absorption (298 K) λ_{abs} (nm)[a]	Emission λ_{em} (nm) 298 K/77 K	Φ_p (%)[b]	τ_p (μs)[c]	$\Delta T_{5\%}/T_g$ (°C)[d]
1	303 (4.36), 364 (4.23), 382 (4.26), 415 (4.18) 435 (4.21)	498, 569, 628[e]/468, 573, 625[e]	3.9	58.3	305/176
2	305 (4.49), 368 (4.29), 387 (4.34), 423 (4.36) 440 (4.40)	516, 570[e], 632[e]/475, 575, 623[e]	8.6	54.6	303/175
3	311 (4.36), 326 (4.43), 363[e] (3.92), 405 (3.82) 422 (3.80)	538, 582[e], 624[e]/541, 588[e], 619[e]	16.8	25.0	301/136

[a] Measured in CH_2Cl_2 at a concentration of 10^{-5} M and logε values are shown in parentheses.
[b] In degassed CH_2Cl_2 relative to *fac*-[Ir(ppy)$_3$] ($\Phi_p = 0.40$), $\lambda_{ex} = 400$ nm.
[c] Measured at 77 K in CH_2Cl_2 at a concentration of 10^{-5} M for the solution samples, and the excitation wavelength was set at 337 nm.
[d] $\Delta T_{5\%}$ is the 5% weight-reduction temperature and T_g is the glass-transition temperature.
[e] Shoulder band.

two emission bands to arise from the same species (see Supporting Information). Complex **2** shows a similar PL behavior to that of **1** at both rt and 77 K. At rt, the emission band fluoresces at 516 nm with a lifetime of 2.46 ns accompanied by a phosphorescence shoulder peak. Because of the much closer energy level between the ILCT and the LC $^3\pi$–π^* states, the triplet emission appeared only as an unconspicuous shoulder on the ILCT emission. The structured luminescence profile of **3** corresponds to the typical stretching modes of the aromatic ligand which is diagnostic of the involvement of the LC $^3\pi$–π^* transition in the emission, and its vibronic pattern likely precludes the assignment of MLCT states that are usually broad and featureless. When the size of the cyclometalating organic group increases by attaching the diarylamino functional group to the fluorenylpyridine ligand, the Pt(II) center would be anticipated to show a lessened spin–orbital coupling interaction in **1** and **2** relative to **3**, presumably because of extended delocalization of the HOMO and lack of Pt participation in the transition state. As a result, both LC fluorescence and phosphorescence can be observed in the PL spectrum of **1** and **2** at rt [26]. Low-temperature PL spectra were also recorded for **1**–**3** at 77 K and they are all essentially dominated by the intense phosphorescence bands in frozen CH_2Cl_2 at the expense of the higher-lying singlet emissions. Furthermore, the relatively long lifetimes for **1**–**3** at 77 K ($\tau_p = 58.3$ μs for **1**, 54.6 μs for **2** and 25.0 μs for **3**) confirm the LC $^3\pi$–π^* states instead of ^{3}MLCT states. Attachment of different R groups does not seem to alter the phosphorescent emission energies of **1** and **2**. Presumably, the singlet state may be described as an zwitterionic species and so the inductive effect is consistent with the shift observed. For the phosphorescence, the triplet state is better described as a diradical, and so the inductive effect is much less felt and not much shifting would be anticipated [27]. Also, by looking at the fluorescence band, we see no vibronic structure while the phosphorescence has some. This suggests that there may be a twist charge transfer phenomenon where a twist angle changes much in the singlet state [28].

The thermal properties of **1**–**3** were characterized by thermogravimetric analysis (TGA) and differential scanning calorimetry (DSC). All the Pt complexes are thermostable up to ca. 300 °C. Complexes **1** and **2** show higher glass-transition temperatures ($T_g \sim 175$ °C) than that of **3** (136 °C). These data are highly desirable for OLEDs of high stability and efficiency. We contend that the 9-substituted fluorene moiety will be mainly responsible for conferring the amorphous properties to the complexes while the diarylamino unit plays a crucial role in improving T_g.

2.5. Electrochemical and electronic characterization

The electrochemical properties of **1**–**3** were examined using cyclic voltammetry (Table 3). All of them show a quasi-reversible reduction couple between −2.42 and −2.46 V, which is consistent with the pyridyl character for the LUMOs of these complexes (Fig. 2). Complexes **1** and **2** show two quasi-reversible oxidation waves (0.32 and 0.48 V for **1**, 0.26 and 0.39 V for **2**), which can be assigned to the oxidation of the electron-rich diarylamino ligand rather than the metal-localized oxidation since the Pt(II) redox process is usually irreversible [19]. While complex **3** exhibits only one irreversible oxidation wave at ca. 0.49 V, this event is probably caused by the oxidation of metal ion [19], because the cyclometalating ligand in **3** lacks the diarylamine moiety and as a result is more difficult to be oxidized as compared to **1** and **2**. When the diarylamino end group is attached to the fluorene ring, each of **1** and **2** can show an elevated HOMO energy level (−5.12 eV for **1** and −5.06 eV for **2**) relative to **3** (−5.29 eV), indicating that compounds **1** and **2** are more electropositive (or have a lower ionization potential) than the non-arylamine capped analogue, and a better HT ability in **1** and **2** can be expected. In other words, the diarylamino capping group has the function of facilitating the HI/HT characteristics of these bifunctional triplet emitters.

Table 3
Redox properties of **1**–**3**

Complex	$E_{1/2}^{ox}$ (V)[a]	$E_{1/2}^{red}$ (V)[a]	HOMO (eV)	LUMO (eV)
1	0.32, 0.48	−2.44	−5.12	−2.36
2	0.26, 0.39	−2.42	−5.06	−2.38
3	0.49[b]	−2.46	−5.29	−2.34

[a] 0.1 M $[Bu_4N]PF_6$ in CH_2Cl_2, scan rate 100 mV s^{-1}, vs. F_c/F_c^+ couple.
[b] Irreversible wave.

2.6. Electrophosphorescent OLED characterization

To illustrate the electrophosphorescent ability and light-emitting performance in optoelectronic applications, the OLEDs with triplet emitter **1** doped in different organic hosts were fabricated and characterized. Firstly, 3,5-dicarbazolylbenzene (mCP) was chosen as the host material for the excellent overlap between the UV–Vis absorption of **1** with the PL spectrum of mCP and the devices were made in the configuration of ITO/NPB/x% Pt:mCP/TPBI/LiF/Al (Fig. 4). 4,4′-Bis[*N*-(1-naphthyl)-*N*-phenylamino]biphenyl (NPB) layer is the HT layer. 2,2′,2″-(1,3,5-Phenylene)tris(1-phenyl-1*H*-benzimidazole) (TPBI) behaves as both a hole-blocker (HBL) and an electron-transporter (ETL). LiF acts as an electron-injection layer and aluminum as the cathode. TPBI, which has a higher electron mobility than the common materials such as 2,9-dimethyl-4,7-diphenyl-1,10-phenanthroline (BCP) and tris(8-hydroxyquinoline) (Alq_3), was used to confine excitons within the emissive zone. The HOMO (−5.12 eV) and LUMO (−2.36 eV) levels in **1** closely match the energy levels for NPB (HOMO: −5.2 eV) and mCP (HOMO: −5.8 eV, LUMO: −2.3 eV). To optimize the device efficiency, concentration dependence experiment was carried out in the doping range between 1 and 12 wt.% (devices **A**–**D**). In the present work, no emission from mCP was observed for all doping levels of complex **1** even at high current density, indicating an effective energy transfer from

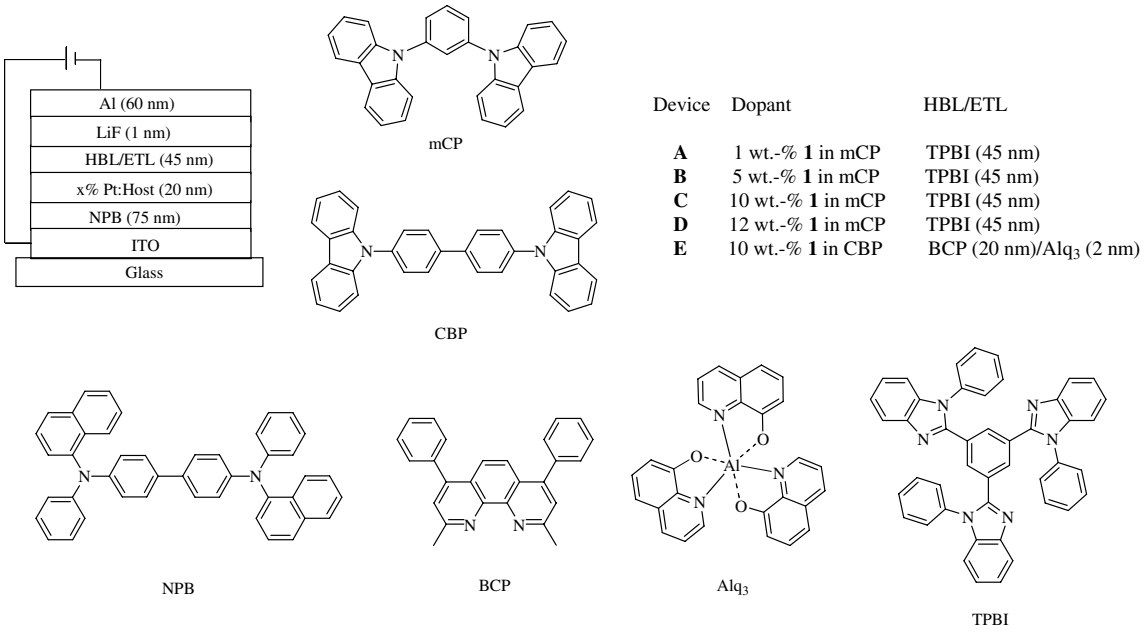

Fig. 4. The general structure of OLEDs and the chemical structure of the compounds used in these devices.

the host exciton to the platinum phosphor upon electrical excitation and the effective hole-blocking of TPBI. There is no sign of metal complex aggregation in the fabricated devices. Fig. 5 shows the EL spectra of these devices at a driving voltage of 8 V. From the vibronic progressions of the spectra, the EL emission should mainly come from the LC $^3\pi$–π^* states. Gratifyingly, we note that the maximum EL peak, spectral profile and the Commission Internationale de L'Eclairage (CIE) color coordinates are almost invariant of the guest concentration in each case, and no additional excimeric band was observed. This is in contrast to many other devices based on similar platinum emitters which often show monomeric and excimeric dual emissions even at low doping concentration due to the exhibition of π–π stacking and metal–metal interactions between adjacent molecules [11,19]. Furthermore, apart from the $^3\pi$–π^* phosphorescence, there is no emission for the high-lying LC fluorescence in its EL spectra, which might be due to the effective energy transfer between the two emitting states. These results suggest that a new avenue can be developed to ensure a good purity of emission color of Pt phosphors by eliminating such drawbacks as strong intramolecular interactions and poor emitting color purity of the cyclometalated Pt(β-diketonato) complexes.

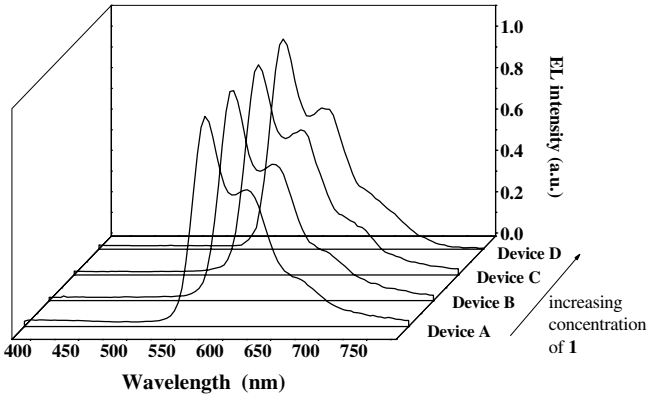

Fig. 5. Concentration dependence of the EL spectra of **1**-doped OLEDs **A**–**D** at 8 V under different dopant concentrations with mCP as the host.

Basically, each of the devices **A**–**D** exhibits a strong orange EL peak at about 570 nm with turn-on voltages ($V_{\text{turn-on}}$) of 5.6–6.7 V for brightness at 1 cd/m^2. The key performance characteristics of the devices **A**–**D** are summarized in Table 4. Fig. 6 presents current density–voltage–luminance (*J*–*V*–*L*) curves of the Pt-doped devices **A**–**D**. The luminance of the devices **A**–**D** reached 3158–4834 cd/m^2 at 15 V. The best device performance is achieved at the doping level of 5 wt.% (device **B**). At 7 V, device **B** achieved the external quantum efficiency (η_{ext}) of 4.65% photons/electron (ph/el), current efficiency (η_{L}) of 11.75 cd/A and power efficiency (η_{p}) of 5.27 lm/W. Although the dependence of EL color on the dopant level of other square-planar Pt complexes has been reported, in which the spectra displayed both the monomeric and aggregated EL peaks with different relative intensities upon variation of the dopant concentration, our results show that complex **1** is suitable for the realization of single-color EL devices by virtue of the bulkiness of the complex. Plots of the device efficiencies as a function of current density for **A**–**D** are depicted in Fig. 7. As is the case for other electrophosphorescent devices, the device efficiencies witnessed decay with increasing driving voltage and current density. The decrease has been ascribed to a combination of triplet–triplet annihilation of the phosphor-bound excitons [29] and field-induced quenching effects [30].

In order to optimize the device performance further, CBP was also employed as the triplet host for fabricating

Table 4
Performance of **1**-doped electrophosphorescent OLEDs

Device	Phosphor dopant	$V_{turn\text{-}on}$ (V)	Luminance L (cd/m^2)[a]	η_{ext} (%)	η_L (cd/A)	η_p (lm/W)	λ_{max} (nm)[d]
A	**1** (1 wt.%)	5.6	3158 (15)	4.39 (7)[a]	11.40 (7)	4.89 (7)	568
				4.19[b]	10.89	4.42	(0.53, 0.46)
				1.44[c]	3.75	1.10	
B	**1** (5 wt.%)	6.2	4834 (15)	4.65 (7)[a]	11.75 (7)	5.27 (7)	572
				4.10[b]	10.13	3.92	(0.54, 0.46)
				2.40[c]	6.08	1.80	
C	**1** (10 wt.%)	6.7	3371 (15)	4.18 (8.5)[a]	10.04 (8.5)	3.71 (8.5)	572
				3.92[b]	9.39	3.17	(0.55, 0.45)
				1.88[c]	4.15	1.17	
D	**1** (12 wt.%)	6.5	3540 (15)	3.55 (7)[a]	8.98 (7)	4.03 (7)	572
				3.11[b]	8.76	2.84	(0.55, 0.45)
				1.67[c]	4.23	1.17	
E	**1** (10 wt.%)	5.3	4195 (15)	6.64 (7.5)[a]	15.41 (7.5)	7.07 (7.5)	572
				6.60[b]	15.30	6.03	(0.55, 0.45)
				4.45[c]	10.31	2.87	

[a] Maximum values of the devices. Values in parentheses are the voltages at which they were obtained.
[b] Values collected at 100 cd/m^2.
[c] Values collected at 1000 cd/m^2.
[d] CIE coordinates [x, y] in parentheses.

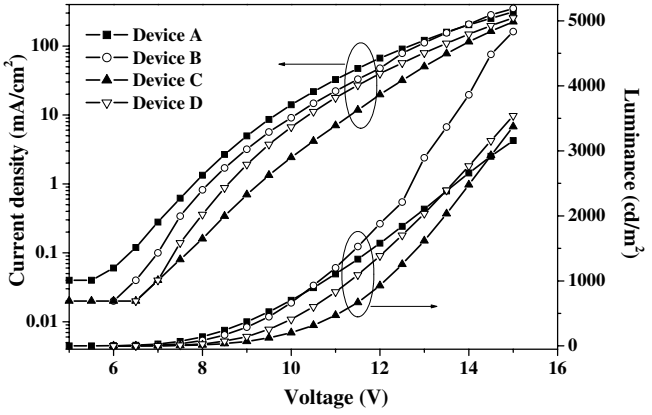

Fig. 6. The current density–voltage–luminance (J–V–L) characteristics of devices **A**–**D**.

the OLEDs with the configuration ITO/NPB/x% Pt:CPB/BCP/Alq_3/LiF/Al using a combination of BCP/Alq_3 as the alternative layer instead of TPBI for the best results, typical for Ir(ppy)$_3$-type compounds (Hppy = 2-phenylpyridine). BCP is used as the hole-blocking material and Alq_3 serves as the electron-transporter. Our results show that the optimum device performance is achieved at the doping level of 10 wt.% (device **E**) with a turn-on voltage of 5.3 V, a maximum luminance of 4195 cd/m^2 at 15 V, η_{ext} of 6.64% at 7.5 V, η_L of 15.41 cd/A at 7.5 V, and η_p of 7.07 lm/W at 6.5 V (Table 5). The J–V–L characteristics, EL spectrum and the efficiency curves of device **E** are shown in Figs. 8–10, respectively. Device **E** shows a similar EL spectrum with that of device **B,** the best device with mCP host. We observe that device **E** outperforms that of device **B** and its EL spectrum is also dominated by the LC $^3\pi$–π^* emission at $\lambda_{max} = 570$ nm. The lower triplet energy of CBP ($\lambda_{max} \sim 460$ nm) [31] compared with that of mCP ($\lambda_{max} \sim 410$ nm) [11,32] ensures a more efficient energy transfer for the triplet of CBP to the LC $^3\pi$–π^* states of **1**.

On the other hand, WOLEDs have also drawn much recent attention in the academic and industrial R&D sectors because of their potential use in display backlights, full color applications, as well as in solid-state lighting purposes [11,12,33]. But most WOLEDs utilize emission from several different colored emitters in separate layers to avoid

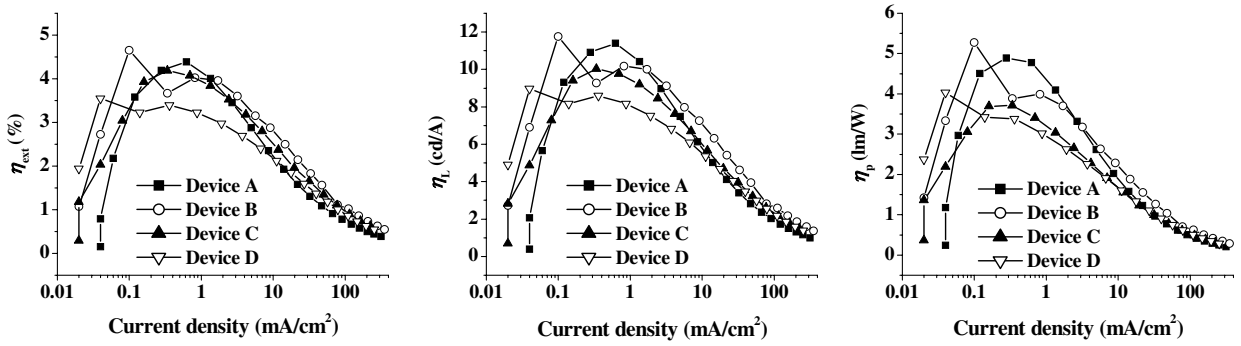

Fig. 7. The efficiencies of the devices **A**–**D** as a function of current density.

Table 5
Summary of crystal structure data for **1**–**3**

	1 · $CHCl_3$	**2**	**3**
Formula	$C_{40}H_{37}Cl_3N_2O_2Pt$	$C_{41}H_{40}N_2O_2Pt$	$C_{27}H_{27}NO_2Pt$
M_r	879.16	787.84	592.59
crystal size (mm)	$0.30 \times 0.19 \times 0.17$	$0.32 \times 0.24 \times 0.22$	$0.28 \times 0.25 \times 0.20$
Crystal system	Monoclinic	Monoclinic	Monoclinic
Space group	$P2_1/c$	$P2_1/c$	$P2_1/c$
a (Å)	24.1106(15)	9.7385(5)	8.1679(5)
b (Å)	13.6691(9)	11.2842(5)	26.7111(15)
c (Å)	13.1241(8)	31.6544(15)	10.9458(6)
α (°)	90	90	90
β (°)	90.2780(10)	94.9410(10)	107.2510(10)
γ (°)	90	90	90
V (Å^3)	4325.3(5)	3465.6(3)	2280.7(2)
Z	4	4	4
D_{calc} (g cm^{-3})	1.350	1.510	1.726
μ (mm^{-1})	3.461	4.086	6.176
$F(000)$	1744	1576	1160
2θ Range (°)	2.25–25.00	2.10–28.27	2.47–28.30
Number of reflections collected	20919	20129	13355
Number of unique reflections	7563	7979	5267
R_{int}	0.0344	0.0206	0.0232
Number of reflections with $I > 2.0\sigma(I)$	5598	6760	4382
Number of parameters	469	415	280
R_1, wR_2 $[I > 2.0\sigma(I)]$[a]	0.0422, 0.1168	0.0307, 0.0710	0.0272, 0.0616
R_1, wR_2 (all data)[a]	0.0648, 0.1322	0.0394, 0.0742	0.0309, 0.0628
Goodness-of-fit on F^2[b]	1.070	1.082	1.176

[a] $R_1 = \sum\|F_o| - |F_c\|/\sum|F_o|$. $wR_2 = \{\sum [w(F_o^2 - F_c^2)^2]/\sum [w(F_o^2)^2]\}^{1/2}$.
[b] $\text{GoF} = [(\sum w|F_o| - |F_c|)^2/(N_{obs} - N_{param})]^{1/2}$.

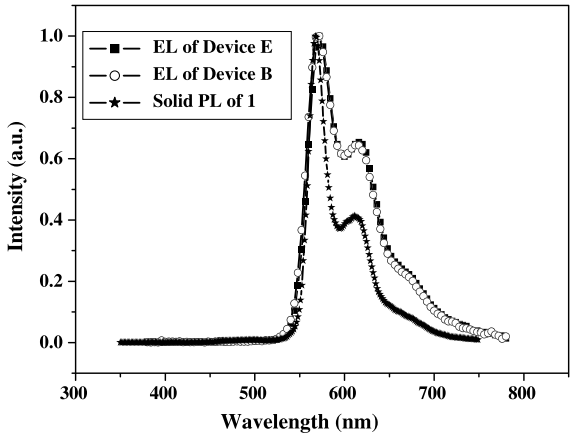

Fig. 8. The EL spectra of device **E** with CBP as the host (the EL of device **B** and solid-state PL of **1** are included in the inset).

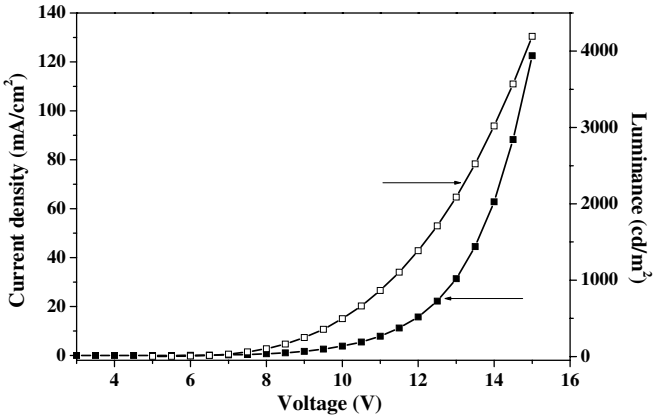

Fig. 9. The current density–voltage–luminance (J–V–L) curves of device **E**.

the ready energy transfer from the higher energy dye to the lower energy dye and achieve a well-balanced emission color. Therefore, this will complicate the device structure and fabrication process. Additionally, in order to realize the generation of white EL that is not driven by varying the bias voltage, we obtained here a simple WOLED through a control of the extent of energy transfer from the blue host 9,10-di(2-naphthyl)anthracene (ADN) [34] to the orange dopant **1** in a configuration similar to that of devices **A**–**E** by replacing mCP or CBP with ADN. A near-white emission is produced by the simultaneous EL of both the blue host and triplet excitons of the dopant (Fig. 11). The CIE coordinates of this device is (0.34, 0.39), which is very close to that of ideal white point of (0.33, 0.33). While preliminary results indicate that the EL efficiency is not yet attractive (<0.2% ph/el or 0.4 cd/A) because of the low triplet energy of ADN and hence less efficient energy transfer to the dopant, such a strategy would be useful for obtaining WOLEDs in a single dopant configuration, in contrast to most examples of white phosphorescent OLEDs that require dual or multiple dopants in multilayer devices. More detailed work on this

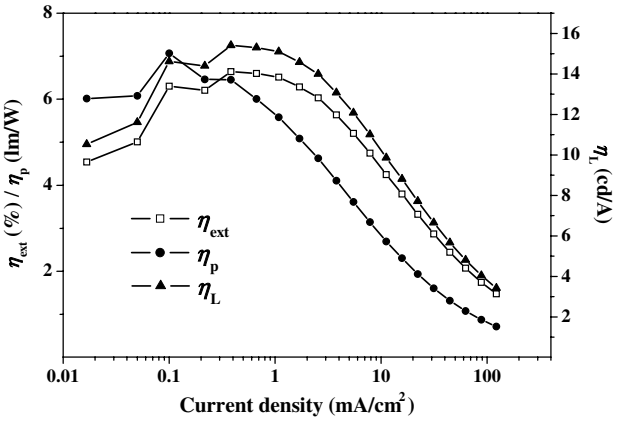

Fig. 10. The dependence of EL efficiencies of device **E** on current density.

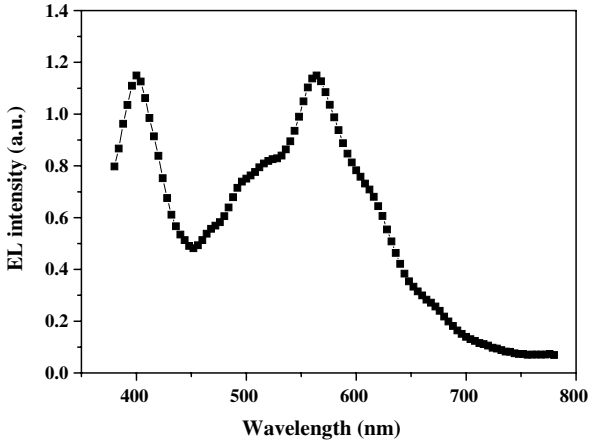

Fig. 11. The EL spectrum of WOLED prepared using complex **1** in the ADN host.

aspect is still ongoing for the eventual realization of white light sources.

3. Conclusions

In summary, the present work reports the synthesis and characterization of some new light-emitting cyclometalated complexes of platinum(II) incorporating both hole-transporting arylamine and light-emitting fluorene moieties, study of their photophysical properties, single-crystal X-ray structural analyses and their applications in monochromatic and white OLEDs. Saliently, end-capping of the fluorene-based metal phosphors with the sterically hindered NAr_2 chromophore can offer advantages in terms of lowering the first ionization potential, which can improve the hole-transporting properties as well as suppressing excimer formation. Due to the multi-component ligand structure, we can successfully circumvent the drawbacks of aggregate formation among the phosphor molecules as revealed from X-ray diffraction studies and suppress the unwanted intermolecular interactions of the dopant that would otherwise cause concentration-dependent spectral changes. In this way, it enables us to prepare pure orange-emitting OLEDs of high performance. After optimization of the fabrication conditions, all the devices emit an intense orange light at about 570 nm with very stable CIE color coordinates and the best device shows an external quantum efficiency of 6.64% corresponding to current and power efficiencies of 15.41 cd/A and 7.07 lm/W. Additionally, these bifunctional platinum phosphors should have the potential to excel in the development of WOLEDs through a wise combination with an appropriate blue host or emitter. Management of the relative EL intensities of the blue host/emitter and the dopant can be a valuable tool for making single-dopant WOLEDs.

4. Experimental

4.1. General procedures

All reactions were performed under nitrogen. Solvents were carefully dried and distilled from appropriate drying agents prior to use. Commercially available reagents were used without further purification unless otherwise stated. The procedure for the synthesis of (7-bromo-9,9-diethylfluoren-2-yl)diphenylamine followed the methods reported in the literature [35]. All reactions were monitored by thin-layer chromatography (TLC) with Merck pre-coated glass plates. Compounds were visualized with UV light irradiation at 254 and 365 nm. Flash column chromatography and preparative TLC were carried out using silica gel from Merck (230–400 mesh) at rt. UV–Vis spectra were obtained on a HP-8453 spectrophotometer. The photoluminescent properties and lifetimes of the compounds were probed on the Photon Technology International (PTI) Fluorescence Master Series QM1 system. The phosphorescence quantum yields were determined in CH_2Cl_2 solutions at 298 K against *fac*-[Ir(ppy)$_3$] as a reference ($\Phi = 0.40$) [36]. Fast-atom bombardment (FAB) mass spectra were recorded on a Finnigan MAT SSQ710 system. NMR spectra were measured in $CDCl_3$ on a Varian Inova 400 MHz FT-NMR spectrometer; chemical shifts were quoted relative to the internal standard tetramethylsilane for ^1H and $^{13}C\{^1H\}$ NMR data. Thermal analyses were performed with the Perkin–Elmer Pyris Diamond DSC and Perkin–Elmer TGA6 thermal analyzers. Cyclic voltammetry was performed using an EG&G potentiostat model 283. Anhydrous THF was used as the solvent under a nitrogen atmosphere, and 0.1 M tetra(*n*-butyl)ammonium hexafluorophosphate was used as the supporting electrolyte. A Pt wire was used as the pseudo-reference electrode, and a Pt sheet was used as the counter electrode. The working electrode was glassy carbon. The redox potentials were reported relative to a ferrocene/ferrocenium (Cp_2Fe/Cp_2Fe^+) redox couple used as an internal standard [37]. The oxidation (E_{ox}) and reduction (E_{red}) potentials were used to determine the HOMO and LUMO energy levels using the equations $E_{HOMO} = -(E_{ox} + 4.8)$ eV and $E_{LUMO} = -(E_{red} + 4.8)$ eV which were calculated using the internal standard ferrocene value of -4.8 eV with respect to the vacuum level [38]. DFT calculations at the

B3LYP level were performed based on their experimental geometries from the X-ray data. The basis set used for C, O, N and H atoms was 6-31G while effective core potentials with a LanL2DZ basis set were employed for Pt [39]. All the calculations were performed with the GAUSSIAN 03 package. For the OLED fabrication and measurements, commercial indium tin oxide (ITO)-coated glass with sheet resistance of 20–30 Ω/square was used as the starting substrate. Before device fabrication, the ITO glass substrates were cleaned by ultrasonic baths in organic solvents followed by ozone treatment for 10 min. Each of the orange-emitting devices was assembled in the following sequence: ITO on glass substrate (anode), 75 nm of NPB, 20 nm of the emitting layer made of the organic host (mCP or CBP) and phosphorescent Pt dopant (x%), 45 nm of TPBI or 20 nm of BCP followed by 2 nm of Alq_3, 1 nm of LiF, and 60 nm of Al (cathode). The organic layers were evaporated and laminated in the above sequence under 4×10^{-4} Pa without breaking vacuum between each vacuum deposition process. The emissive layer was formed by co-deposition of the dopant and the host. The layer thickness was monitored in situ using a quartz crystal oscillator. The active area of the device was 5 mm^2 as defined by the shadow mask. The electrical and optical characteristics of these devices were measured using R6145 DC voltage–current source, FLUKE 45 dual display multimeter and Spectrascan PR650 spectrophotometer in a dark room under ambient air condition.

4.2. Preparations of complexes

The syntheses of the cyclometalating ligands are given in the Supporting Information.

4.2.1. Synthesis of (1)

Under a N_2 atmosphere, **HL_1** (0.50 g, 1.07 mmol) and K_2PtCl_4 (0.28 g, 0.67 mmol) were added to a 2-ethoxyethanol/water mixture (15 mL, 3:1, v/v). The reaction mixture was stirred at 80 °C for 16 h. After it was cooled to rt, the reaction mixture was poured into water (200 mL). A yellow precipitate appeared which was collected and dried under vacuum to give the chloro-bridged dimer as a yellow solid that was used for the next step without further purification. The Pt dimer (0.40 g, 0.29 mmol), Na_2CO_3 (0.60 g, 5.66 mmol) and acetylacetone (0.2 mL) were added to 2-ethoxyethanol (10 mL) under a N_2 atmosphere. The reaction temperature was kept at 100 °C for 16 h. After reaction, it was cooled to rt and water (50 mL) was added. The yellow precipitate was collected and dried. It was then purified by column chromatography with CH_2Cl_2/hexane (1:1, v/v) as eluent. The product was obtained as a bright orange solid (0.05 g, 11%). ^{1}H NMR ($CDCl_3$): δ 8.97 (d, $J = 5.1$ Hz, 1H, Ar), 7.87–7.62 (m, 3H, Ar), 7.33–6.97 (m, 15H, Ar), 5.49 (s, 1H, acac), 2.05 (s, 3H, Me), 2.01 (s, 3H, Me), 1.97–1.87 (m, 4H, Et), 0.37 (t, $J = 7.3$ Hz, 6H, Et). ^{13}C NMR ($CDCl_3$): δ 185.74, 184.10, 168.49, 152.04, 148.05, 147.24, 145.33, 142.88, 142.49, 137.86, 136.95, 129.12, 128.27, 123.86, 123.44, 122.40, 121.10, 120.81, 120.39, 118.99, 118.51, 117.35 (Ar), 102.51 (acac CH), 55.65 (quat. C), 32.88, 32.45, 28.30, 8.57 (Et + Me). FAB-MS (m/z): 759 [M^+]. Anal. Calc. for $C_{39}H_{36}N_2O_2Pt$: C, 61.65; H, 4.78; N, 3.69. Found: C, 61.56; H, 4.55; N, 3.40%.

4.2.2. Synthesis of (2)

The complex was synthesized from **HL_2** by a similar protocol as above for **1**, and it was isolated as an orange powder in an overall yield of 15%. ^{1}H NMR ($CDCl_3$): δ (ppm) 8.97 (d, $J = 4.8$ Hz, 1H, Ar), 7.84 (s, 1H, Ar), 7.77–7.74 (m, 1H, Ar), 7.65–7.60 (m, 2H, Ar), 7.33 (s, 1H, Ar), 7.07–6.94 (m, 10H, Ar), 6.95 (dd, $J = 8.0$, 2.0 Hz, 1H, Ar), 5.49 (s, 1H, acac), 2.32 (s, 6H, Me), 2.05 (s, 3H, acac), 2.01 (s, 3H, acac), 1.98–1.86 (m, 4H, Et), 0.36 (t, $J = 7.6$ Hz, 6H, Et). ^{13}C NMR ($CDCl_3$): δ (ppm) 185.71, 184.08 (acac CO), 168.50, 151.87, 147.68, 147.17, 145.64, 145.21, 143.09, 142.18, 137.83, 137.57, 136.04, 131.94, 129.72, 124.09, 122.29, 120.94, 120.59, 120.29, 118.10, 117.77, 117.32 (Ar), 102.51 (acac CH), 55.59 (quat. C), 32.89, (Et), 28.31, 27.21 (acac Me), 20.80 (Me), 8.57 (Et). FAB-MS (m/z): 787 [M^+]. Anal. Calc. for $C_{41}H_{40}N_2O_2Pt$: C, 62.50; H, 5.12; N, 3.56. Found: C, 62.34; H, 5.02; N, 3.40%.

4.2.3. Synthesis of (3)

This compound was prepared similarly from **HL_3** and it was isolated as a yellow–orange solid in 35% yield. ^{1}H NMR ($CDCl_3$): δ 9.00 (d, $J = 5.6$ Hz, 1H, Ar), 7.97 (s, 1H, Ar), 7.82–7.77 (m, 2H, Ar), 7.69 (d, $J = 8.0$ Hz, 1H, Ar), 7.39 (s, 1H, Ar), 7.35–7.30 (m, 3H, Ar), 7.10–7.06 (m, 1H, Ar), 5.51 (s, 1H, acac), 2.08–2.02 (m, 10H, Et + Me), 0.33 (t, $J = 7.4$ Hz, 6H, Et). ^{13}C{^{1}H} NMR ($CDCl_3$): δ 185.72, 184.10, 168.39, 150.59, 147.23, 145.33, 143.27, 143.03, 141.74, 137.92, 137.41, 127.09, 126.65, 122.59, 121.29, 120.63, 120.41, 118.29, 117.46 (Ar), 102.55 (acac CH), 55.67 (quat. C), 32.68, 28.32, 27.21, 8.55 (Et + Me). MS (FAB) m/z: 592 [M^+]. Anal. Calc. for $C_{27}H_{27}NO_2Pt$: C, 54.72; H, 4.59; N, 2.36. Found: C, 54.59; H, 4.75; N, 2.12%.

5. X-ray crystallography

Diffraction data were collected at 293 K using graphite monochromated Mo Kα radiation ($\lambda = 0.71073$ Å) on a Bruker Axs SMART 1000 CCD diffractometer. The collected frames were processed with the software SAINT+ [40] and an absorption correction (SADABS) [41] was applied to the collected reflections. The structure was solved by the Direct methods (SHELXTL) [42] in conjunction with standard difference Fourier techniques and subsequently refined by full-matrix least-squares analyses on F^2. Hydrogen atoms were generated in their idealized positions and all non-hydrogen atoms were refined anisotropically. Table 5 contains some pertinent crystal data for **1**–**3**.

Acknowledgements

W.-Y.W. thanks the Hong Kong Research Grants Council (Grant No.: HKBU202106) and Hong Kong Baptist University (FRG/04-05/II-59) for the financial support of this work.

Appendix A. Supplementary material

CCDC 639790, 639791 and 639792 contain the supplementary crystallographic data for this paper. These data can be obtained free of charge via http://www.ccdc.cam.ac.uk/conts/retrieving.html, or from the Cambridge Crystallographic Data Centre, 12 Union Road, Cambridge CB2 1EZ, UK; fax: (+44) 1223-336-033; or e-mail: deposit@ccdc.cam.ac.uk. Supplementary data associated with this article can be found, in the online version, at doi:10.1016/j.jorganchem.2007.04.013.

References

[1] (a) V. Balzani, A. Credi, F. Scandola, L. Fabbrizzi, A. Poggi (Eds.), Transition Metals in Supramolecular Chemistry, Kluwer, Dordrecht, The Netherlands, 1994;
(b) J.M. Lehn, Supramolecular Chemistry – Concepts and Perspectives, VCH, Weinheim, Germany, 1995;
(c) C.A. Bignozzi, J.R. Schoonover, F. Scandola, Prog. Inorg. Chem. 44 (1997) 1;
(d) R.C. Evans, P. Douglas, C.J. Winscom, Coord. Chem. Rev. 250 (2006) 2093;
(e) E. Holder, B.M.W. Langeveld, U.S. Schubert, Adv. Mater. 17 (2005) 1109.

[2] (a) Y.-L. Tung, S.-W. Lee, Y. Chi, L.-S. Chen, C.-F. Shu, F.-I. Wu, A.J. Carty, P.-T. Chou, S.-M. Peng, G.-H. Lee, Adv. Mater. 17 (2005) 1059;
(b) M. Grätzel, Nature 414 (2001) 338.

[3] (a) Y.-H. Niu, Y.-L. Tung, Y. Chi, C.-F. Shu, J.H. Kim, B. Chen, J. Luo, A.J. Carty, A.K.-Y. Jen, Chem. Mater. 17 (2005) 3532;
(b) X. Jiang, A.K.-Y. Jen, B. Carlson, L.R. Dalton, Appl. Phys. Lett. 81 (2002) 3125;
(c) B. Carlson, G.D. Phelan, W. Kaminsky, L. Dalton, X.Z. Jiang, S. Liu, A.K.-Y. Jen, J. Am. Chem. Soc. 124 (2002) 14162;
(d) Y. Ma, H. Zhang, J. Shen, C. Che, Synth. Met. 94 (1998) 245;
(e) Y.-L. Tung, S.-W. Lee, Y. Chi, Y.-T. Tao, C.-H. Chien, Y.-M. Cheng, P.-T. Chou, S.-M. Peng, C.-S. Liu, J. Mater. Chem. 15 (2005) 460;
(f) P.-T. Chou, Y. Chi, Eur. J. Inorg. Chem. (2006) 3319.

[4] (a) V.W.-W. Yam, Chem. Commun. (2001) 789;
(b) K.K.-W. Lo, W.-K. Hui, D.C.-M. Ng, J. Am. Chem. Soc. 124 (2002) 9344.

[5] (a) S.-J. Yeh, M.-F. Wu, C.-T. Chen, Y.-H. Song, Y. Chi, M.-H. Ho, S.-F. Hsu, C.H. Chen, Adv. Mater. 17 (2005) 285;
(b) C.-L. Li, Y.-J. Su, Y.-T. Tao, P.-T. Chou, C.-H. Chien, C.-C. Cheng, R.-S. Liu, Adv. Funct. Mater. 15 (2005) 387;
(c) D.K. Rayabarapu, B.M.J.S. Paulose, J.-P. Duan, C.-H. Cheng, Adv. Mater. 17 (2005) 349;
(d) Y.-H. Song, S.-J. Yeh, C.-T. Chen, Y. Chi, C.-S. Liu, J.-K. Yu, Y.-H. Hu, P.-T. Chou, S.-M. Peng, G.-H. Lee, Adv. Funct. Mater. 14 (2004) 1221;
(e) H.Z. Xie, M.W. Liu, O.Y. Wang, X.H. Zhang, C.S. Lee, L.S. Hung, S.T. Lee, P.F. Teng, H.L. Kwong, H. Zheng, C.M. Che, Adv. Mater. 13 (2001) 1245;
(f) J.M. Lupton, I.D.W. Samuel, M.J. Frampton, R. Beavington, P.L. Burn, Adv. Funct. Mater. 11 (2001) 287.

[6] (a) I.M. Dixon, J.P. Collin, J.P. Sauvage, L. Flamigni, S. Encinas, F. Barigelletti, Chem. Soc. Rev. 29 (2000) 385;
(b) W.J. Finkenzeller, H. Yersin, Chem. Phys. Lett. 377 (2003) 299;
(c) C.-L. Lee, R.R. Das, J.-J. Kim, Chem. Mater. 16 (2004) 4642;
(d) H.-C. Li, P.-T. Chou, Y.-H. Hu, Y.-M. Cheng, R.-S. Liu, Organometallics 24 (2005) 1329;
(e) K.R. Justin Thomas, M. Velusamy, J.T. Lin, C.-H. Chien, Y.-T. Tao, Y.S. Wen, Y.-H. Hu, P.-T. Chou, Inorg. Chem. 44 (2005) 5677;
(f) W.-S. Huang, J.-T. Lin, C.-H. Chien, Y.-T. Tao, S.-S. Sun, Y.-S. Wen, Chem. Mater. 16 (2004) 2480.

[7] (a) W.-Y. Wong, C.-L. Ho, Z.-Q. Gao, B.-X. Mi, C.-H. Chen, K.-W. Cheah, Z. Lin, Angew. Chem., Int. Ed. 45 (2006) 7800;
(b) G. Zhou, W.-Y. Wong, B. Yao, Z. Xie, L. Wang, Angew. Chem., Int. Ed. 46 (2007) 1149;
(c) W.-Y. Wong, G.-J. Zhou, X.-M. Yu, H.-S. Kwok, Z. Lin, Adv. Funct. Mater. 17 (2007) 315;
(d) X. Yu, H.-S. Kwok, W.-Y. Wong, G.-J. Zhou, Chem. Mater. 18 (2006) 5097.

[8] (a) I.R. Laskar, S.-F. Hsu, T.-M. Chen, Polyhedron 24 (2005) 881;
(b) J. Kavitha, S.-Y. Chang, Y. Chi, J.-K. Yu, Y.-H. Hu, P.-T. Chou, S.-M. Peng, G.-H. Lee, Y.-T. Tao, C.-H. Chien, A.J. Carty, Adv. Funct. Mater. 15 (2005) 223;
(c) W. Lu, B.-X. Mi, M.C.W. Chan, Z. Hui, C.-M. Che, N. Zhu, S.-T. Lee, J. Am. Chem. Soc. 126 (2004) 4958;
(d) S.-C. Chan, M.C.W. Chan, Y. Wang, C.-M. Che, K.-K. Cheung, N. Zhu, Chem. Eur. J. 7 (2001) 4180.

[9] (a) W.-Y. Wong, Z. He, S.-K. So, K.-L. Tong, Z. Lin, Organometallics 24 (2005) 4079;
(b) Z. He, W.-Y. Wong, X.-M. Yu, H.-S. Kwok, Z. Lin, Inorg. Chem. 45 (2006) 10922.

[10] (a) M. Hissler, W.B. Connick, D.K. Geiger, J.E. McGarrah, D. Lipa, R.J. Lachicotte, R. Eisenberg, Inorg. Chem. 39 (2000) 447;
(b) T.J. Wadas, S. Chakraborty, R.J. Lachicotte, Q.-M. Wang, R. Eisenberg, Inorg. Chem. 44 (2005) 2628;
(c) S. Chakraborty, T.J. Wadas, H. Hester, C. Flaschenreim, R. Schmehl, R. Eisenberg, Inorg. Chem. 44 (2005) 6284.

[11] F. Barigelletti, D. Sandrini, M. Maestri, V. Balzani, A. von Zelewsky, L. Chassot, P. Jolliet, U. Maeder, Inorg. Chem. 27 (1988) 3644.

[12] T.K. Aldridge, E.M. Stacy, D.R. Mcmillin, Inorg. Chem. 33 (1994) 722.

[13] J.M. Bevilacqua, R. Eisenberg, Inorg. Chem. 33 (1994) 2913.

[14] V. Adamovich, J. Brooks, A. Tamayo, A.M. Alexander, P.I. Djurovich, B.W. D'Andrade, C. Adachi, S.R. Forrest, M.E. Thompson, New J. Chem. 26 (2002) 1171.

[15] B. D'Andrade, J. Brooks, V. Adamovich, M.E. Thompson, S.R. Forrest, Adv. Mater. 14 (2002) 1032.

[16] W.-Y. Wong, G.-J. Zhou, X.-M. Yu, H.-S. Kwok, B.-Z. Tang, Adv. Funct. Mater. 16 (2006) 383.

[17] J.Q. Ding, J. Gao, Y.X. Cheng, Z.Y. Xie, L.X. Wang, D.G. Ma, X.B. Jing, F.S. Wang, Adv. Funct. Mater. 16 (2006) 575.

[18] B.N. Cockburn, D.V. Howe, T. Keating, B.F.G. Johnson, J. Lewis, J. Chem. Soc., Dalton Trans. (1973) 404.

[19] J. Brooks, Y. Babayan, S. Lamansky, P.I. Djurovich, I. Tsyba, R. Bau, M.E. Thompson, Inorg. Chem. 41 (2002) 3055.

[20] J. Breu, K.-J. Range, A. von Zelewsky, H. Yersin, Acta Crystallogr. C53 (1997) 562.

[21] (a) A.C. Stückl, U. Klement, K.-J. Range, Z. Kristallogr. 208 (1993) 297;
(b) T.J. Giordano, P.G. Rasmussen, Inorg. Chem. 14 (1975) 1628.

[22] M. Ghedini, D. Pucci, A. Crispini, G. Barberio, Organometallics 18 (1999) 2116.

[23] H. Katoh, K. Miki, Y. Kai, N. Tanaka, N. Kasai, Bull. Chem. Soc. Jpn. 54 (1981) 611.

[24] (a) P.J. Low, M.A.J. Paterson, A.E. Goeta, D.S. Yufit, J.A.K. Howard, J.C. Cherryman, D.R. Tackley, B. Brown, J. Mater. Chem. 14 (2004) 2516;

(b) P.J. Low, M.A.J. Paterson, H. Puschmann, A.E. Goeta, J.A.K. Howard, C. Lambert, J.C. Cherryman, D.R. Tackley, S. Leeming, B. Brown, Chem.-Eur. J. 10 (2004) 83.
[25] A. Tsuboyama, H. Iwawaki, M. Furugori, T. Mukaide, J. Kamatani, S. Igawa, T. Moriyama, S. Miura, T. Takiguchi, S. Okada, M. Hoshino, K. Ueno, J. Am. Chem. Soc. 125 (2003) 12971.
[26] Y.-L. Chen, S.-W. Li, Y.-M. Cheng, S.-C. Pu, Y.-S. Yeh, P.-T. Chou, ChemPhysChem 6 (2005) 2012.
[27] N.J. Turro, Modern Molecular Photochemistry, University Science Books, Mill Valley, CA, USA, 1991.
[28] (a) P.D. Harvey, G. Durocher, J. Photochem. 27 (1984) 29;
(b) P.D. Harvey, G. Durocher, Can. J. Spectrosc. 29 (1984) 84.
[29] M.A. Baldo, C. Adachi, S.R. Forrest, Phys. Rev. B 62 (2000) 10967.
[30] J. Kalinowski, W. Stampor, J. Mezyk, M. Cocchi, D. Virgili, V. Fattori, P. Di Marco, Phys. Rev. B 66 (2002) 235321-1.
[31] M.A. Baldo, S.R. Forrest, Phys. Rev. B 62 (2000) 10958.
[32] K. Naito, A. Miura, J. Phys. Chem. 97 (1993) 6240.
[33] (a) Y. Sun, N.C. Giebink, H. Kanno, B. Ma, M.E. Thompson, S.R. Forrest, Nature 440 (2006) 908;
(b) P.-I. Shih, C.-F. Shu, Y.-L. Tung, Y. Chi, Appl. Phys. Lett. 88 (2006) 251110–251111;
(c) A.J. Heeger, Solid State Commun. 107 (1998) 673;
(d) X. Gong, S. Wang, D. Moses, G.C. Bazan, A.J. Heeger, Adv. Mater. 17 (2005) 2053;
(e) G. Tu, C. Mei, Q. Zhou, Y. Cheng, Y. Geng, L. Wang, D. Ma, X. Jing, F. Wang, Adv. Funct. Mater. 16 (2006) 101;
(f) J. Liu, Q. Zhou, Y. Cheng, Y. Geng, L. Wang, D. Ma, X. Jing, F. Wang, Adv. Funct. Mater. 16 (2006) 957;
(g) X. Niu, L. Ma, B. Yao, J. Ding, G. Tu, Z. Xie, L. Wang, Appl. Phys. Lett. 89 (2006), 213508-1.
[34] J. Shi, C.W. Tang, Appl. Phys. Lett. 80 (2002) 3201.
[35] R. Kannan, G.S. He, L. Yuan, F. Xu, P.N. Prasad, A.G. Dombroskie, B.A. Reinhardt, J.W. Baur, R.A. Waia, L.-S. Tan, Chem. Mater. 13 (2001) 1896.
[36] K.A. King, P.J. Spellane, R.-J. Watts, J. Am. Chem. Soc. 107 (1985) 1431.
[37] (a) R.R. Gagné, C.A. Koval, G.C. Lisensky, Inorg. Chem. 19 (1980) 2854;
(b) D.T. Sawyer, A. Sobkowiak, J.L. Roberts Jr., Electrochemistry for Chemists, second ed., John Wiley and Sons, New York, 1995, p. 467.
[38] (a) M. Thelakkat, H.-W. Schmidt, Adv. Mater. 10 (1998) 219;
(b) R.S. Ashraf, M. Shahid, E. Klemm, M. Al-Ibrahim, S. Sensfuss, Macromol. Rapid Commun. 27 (2006) 1454.
[39] (a) W.R. Wadt, P.J. Hay, J. Chem. Phys. 82 (1985) 284;
(b) P.J. Hay, W.R. Wadt, J. Chem. Phys. 82 (1985) 299.
[40] SAINT+, ver. 6.02a, Bruker, Analytical X-ray System Inc., Madison, WI, 1998.
[41] G.M. Sheldrick, SADABS, Empirical Absorption Correction Program, University of Göttingen, Germany, 1997.
[42] G.M. Sheldrick, SHELXTL™, Reference Manual, ver. 5.1, Madison, WI, 1997.